Wavelet Formation in Excitable Cardiac Tissue: The Role of Wavefront-Obstacle Interactions in Initiating High-Frequency Fibrillatory-Like Arrhythmias

Josef M. Starobin, Yuri I. Zilberter, Elizabeth M. Rusnak, and C. Frank Starmer
Departments of Medicine (Cardiology) and Computer Science, Duke University Medical Center, Durham, North Carolina 27710 USA

ABSTRACT High-frequency arrhythmias leading to fibrillation are often associated with the presence of inhomogeneities (obstacles) in cardiac tissue and reduced excitability of cardiac cells. Studies of antiarrhythmic drugs in patients surviving myocardial infarction revealed an increased rate of sudden cardiac death compared with untreated patients. These drugs block the cardiac sodium channel, thereby reducing excitability, which may alter wavefront-obstacle interactions. In diseased atrial tissue, excitability is reduced by diminished sodium channel availability secondary to depolarized rest potentials and cellular decoupling secondary to intercellular fibrosis. Excitability can also be reduced by incomplete recovery between successive excitations. In all of these cases, wavefront-obstacle interactions in a poorly excitable medium may reflect an arrhythmogenic process that permits formation of reentrant wavelets leading to flutter, fibrillation, and sudden cardiac death. To probe the relationship between excitability and arrhythmogenesis, we explored conditions for new wavelet formation after collision of a plane wave with an obstacle in an otherwise homogeneous excitable medium. Formulating our approach in terms of the balance between charge available in the wavefront and the excitation charge requirements of adjacent medium, we found analytically the critical medium parameters that defined conditions for wavefront-obstacle separation. Under these conditions, when a parent wavefront collided with a primitive obstacle, the resultant fragments separated from the obstacle boundaries, subsequently curled, and spawned new "daughter" wavelets. We identified spatial arrangements of obstacles such that wavefront-obstacle collisions leading to spawning of new wavelets could produce high-frequency wavelet trains similar to fibrillation-like arrhythmias.

INTRODUCTION

High-frequency arrhythmias leading to fibrillation and sudden cardiac death are often associated with inhomogeneities (obstacles) in cardiac tissue and reduced excitability of individual cells. However, the link between obstacles, reduced excitability, and arrhythmogenesis remains unclear.

Obstacles and reduced excitability can arise from several different mechanisms. Studies of antiarrhythmic drugs in patients surviving myocardial infarction revealed an increased rate of sudden cardiac death compared with untreated patients (CAST Investigators, 1989). Prior myocardial infarction most probably left a residue of "obstacles" or poorly excitable myocardial regions, whereas the drugs utilized in this study reduced excitability by blockade of the cardiac sodium channel. Studies of atrial cells from patients with atrial disease revealed reduced excitability secondary to depolarized rest potentials (Ten Eick and Singer, 1979), whereas studies of human diseased atrial tissue demonstrated an increased microfibrosis that would hypothetically lead to a loss of side-to-side cellular connections, thereby increasing anisotropy, reducing excitability, and increasing the size of inexcitable regions (Spach and Dolber, 1986). Excitability can also be attenuated by incomplete recovery associated with high rates of excitation (Schalij et al., 1992; Konings et al., 1994). The complex interaction of inhomogeneities and reduced excitability highlighted in these examples with the nonlinear dynamics of cardiac cells may reflect arrhythmogenic conditions that promote formation of wavelets leading to reentrant arrhythmias, fibrillation, and sudden cardiac death.

Reentrant activation (spiral wave) is observed in many excitable preparations (Winfree, 1987, 1989; Zykov, 1988; Davidenko, 1995). Variations of electrocardiographic potentials (ECG) associated with reentrant cardiac tachycardias are synchronous with the rotation of a single spiral (Krinsky, 1984; Markin et al., 1981; Pertsov et al., 1993). Fibrillation, on the other hand, often reflects multiple reentrant wavelets (Allessie et al., 1994; Konings et al., 1994; Cox et al., 1994), leading to high-frequency oscillation of the ECG potential that is not synchronized with rotation of a single spiral.

The initial work of Balakhovsky (1965) and Krinsky (1966) demonstrated that a temporary obstacle, caused by prolonged refractoriness in a localized region of excitable medium, was adequate to rupture an incident wavefront in a manner that led to spiral wave development. Pertsov and co-workers (1983) extended these results in numerical studies of the collisions between a planar wavefront and a permanent obstacle in an otherwise homogeneous medium. As the medium excitability was reduced (as determined by a model parameter similar to the Na conductance), they found that above a critical excitability, the wave fragments remained "attached" to the obstacle borders and immediately reattached proximal to the obstacle. Wave fragments

Received for publication 12 April 1995 and in final form 20 October 1995.
Address reprint requests to C. Frank Starmer, Box 3181, Duke University Medical Center, Durham, NC 27710. Tel.: 919-684-6804; Fax: 919-684-8666; E-mail: cfs@rodney.mc.duke.edu.

0006-3495/96/02/581/14 $2.00

derived from a wavefront colliding with an obstacle when the medium excitability was less than this critical value separated from the obstacle. In these studies, wavebreaks followed by wavefront-obstacle separation could act as a source of new spiral wavelets, as described by Balakhovsky (1965) and Krinsky (1966).

Kogan and colleagues (1990) further explored the role of wavefront-obstacle separation in a series of numerical experiments. As in the Krinsky model (1966), they showed that if the obstacle was "transient" (e.g., physically removed after wavefront collision), then the residual fragments could evolve into counter-rotating spiral wavefronts.

Using high-frequency stimulation to incrementally reduce medium excitability, Panfilov and Keener (1993) extended the Pertsov et al. (1983, 1990) results and showed that obstacle-wavefront separation and spiral wave development displayed "use-dependent" properties. More specifically, if the stimulation rate was fixed such that the interstimulus interval was less than the time necessary for full recovery of excitability, they found that no separation occurred with the first stimulus (wavefront propagated into rested, fully excitable medium); separation but no spiral development occurred with the next few successor stimuli (due to the accumulated loss of excitability); and if the stimulation frequency was high enough, further successor wavefronts fractionated, detached from the object, and evolved into counter-rotating spiral waves (due to the accumulated loss of excitability greater than a critical value). In all of these studies, only single or paired spiral processes were studied.

The observation of multiple propagating wavelets during fibrillation (Allessie et al., 1994, Konings et al., 1994; Schuessler et al., 1995) confirmed an early hypothesis of Moe (1962). Moe and co-workers (1959, 1962, 1964, 1965) proposed the multiple wavelet hypothesis, which explained these high-frequency arrhythmias as a result of repeated wavefront fractionation secondary to inhomogeneities in refractory properties. This hypothesis postulated that high-frequency arrhythmias (e.g., fibrillation) were maintained by multiple interfering wavelets that migrated around inhomogeneous regions such as islets or strands of refractory tissue. Although Moe's studies (Moe et al., 1964) demonstrated that multiple wavelets could be produced by certain combinations of stimulus timing and distributed refractory properties, the mechanism of wavelet formation and maintenance was uncertain. More specifically, after rupture of an incident wavefront after collision with either an obstacle or a refractory region, the conditions that promoted or prevented the formation of independent wavelets were not explored.

Observations of high-frequency arrhythmias in a medium of reduced excitability (Leier et al., 1978; Buxton et al., 1984; Yamashita et al., 1994), combined with medium inhomogeneities, may provide a substrate for formation of multiple wavelets leading to high-frequency arrhythmias. In our opinion, the studies of Krinsky (1966), Pertsov et al. (1983, 1990), Kogan et al. (1990), Panfilov and Keener (1993), and Agladze et al. (1994) all point to a critical role played by wavefront-obstacle separation in new wavelet formation. To date, the relationship between medium parameters and conditions for wavefront-obstacle separation has been limited to modeling different transient time-dependent regimes of medium excitability. In addition, there are no studies that indicate how high-frequency arrhythmias associated with multiple wavelets might arise from a single wavefront propagating in a low-excitability medium.

To explore these issues, we have defined three subproblems that lead from fractionation of a wavefront to a high-frequency arrhythmia:

1) How to spawn a new wavelet after wavefront-obstacle separation;

2) How to insert the newly spawned wavelet behind the parent wavefront;

3) How to multiply wavelet formation.

We explored multiple wavelet formation by first investigating the behavior of the boundary layer between a single obstacle and a colliding wavefront as determined by the balance of charge available in the wavefront and the excitation charge requirements of adjacent medium. Using this approach we found analytical expressions relating critical values of medium parameters to conditions for wavefront-obstacle separation. We approached the question of wavelet formation and transformation of a single wavelet into multiple wavelets leading to fibrillatory-like arrhythmias by exploring spatial arrangements of primitive obstacles in an otherwise homogeneous medium.

MODEL

The normal cardiac action potential duration is approximately 0.3 s, and the excitation wave propagation velocity is approximately 0.5 m s^{-1}. Such rapid propagation makes multiple reentrant wavelets unlikely because the action potential wavelength (approximately 15 cm) can be comparable to the spatial extent of the heart. However, when excitability is diminished as a result of reduced sodium channel availability secondary to Na channel blockade, incomplete recovery from Na channel inactivation secondary to rapid reexcitation, or reduced cellular coupling, the wavelength is reduced so that the spatial requirements for reentry become more probable. In some cases the spatial wavelength may decrease to several millimeters (Spach et al., 1988).

For our numerical and analytical investigations, we used an excitable membrane formulation of the 2D FitzHugh-Nagumo (FitzHugh, 1961) model, describing wave motion, which is given by

$$C_m \frac{\partial u}{\partial t} = \sigma_{Na} f(u) - V + D\left(\frac{\partial^2 u}{\partial x^2} + \frac{\partial^2 u}{\partial y^2}\right)$$

$$\frac{\partial V}{\partial t} = \frac{(\sigma_K u - V)}{\tau_K}.$$

Here σ_{Na},σ_K mimic the maximum sodium and potassium conductances, respectively, and τ_K is a time constant of a

slow recovery process, $I_{Na} = \sigma_{Na} f(u)$ represents an inward excitation current, and $I_K = V$ represents an outward recovery current. To facilitate analyses, we used this system in dimensionless form (Tyson and Keener, 1988; Winfree, 1991):

$$\frac{\partial u}{\partial t} = \frac{\partial^2 u}{\partial x^2} + \frac{\partial^2 u}{\partial y^2} + f(u) - V \quad (1)$$

$$\frac{\partial V}{\partial t} = \epsilon(\gamma u - V), \quad (2)$$

where $u(x,y,t)$ is a dimensionless membrane potential, and $V(x,y,t)$ is a dimensionless slow recovery current. The scale of u is the maximum action potential amplitude U_0, the scale of V is given by $\sigma_{Na}U_0$, the scale of time is $\tau_0 = C_m/\sigma_{Na}$, and the scale of the length L_0 is given by $(D/\sigma_{Na})^{1/2}$. Here C_m is a membrane capacity and D is a diffusion coefficient. The scale factor, γ, is the ratio of slow potassium to fast sodium conductances. The small parameter, ϵ, is equal to $C_m/(\tau_k\sigma_{Na})$.

The function $f(u)$ is the piecewise linear function similar to that used by Starobin et al. (1994) and represents the *i/v* properties similar to those of a membrane sodium current (Fig. 1 *A*). The slope of the right- and left-hand branches of this function, λ, determines the maximum current that is available to depolarize adjoining regions of the excitable medium. Pertsov et al. (1983) used a three-segment piecewise linear $f(u)$ and varied the slope of the middle segment, which is an equivalent way of altering the current available for propagation.

In an otherwise homogeneous medium, we explored conditions for wavefront-obstacle separation resulting from the collision of a plane wave with a simple obstacle. As a first approximation, we have chosen an L-shaped obstacle (Fig. 1 *B*) as a piecewise linear approximation of the proximal aspect of a solid (2D) obstacle that might be encountered in diseased ventricular tissue after infarction. The filament-like nature of the piecewise linear obstacle also approximates micro-fibrotic regions observed in diseased or aged atrial tissue (Spach and Dolber, 1986). We also investigated the interaction of a plane wave with a lattice of L-shaped obstacles. Here, we sought to approximate diffuse disease and investigate the fate of newly spawned wavelets.

The lattice semiperiod, L, and the dimensions of the obstacles were adjusted to investigate the fate of newly spawned wavelets. The boundary conditions for the inexcitable obstacles were "no-flux" conditions, $\partial u/\partial n = 0$, where n is normal to the obstacle boundary. We used periodic boundary conditions for the domain boundaries along the lines of symmetry, A_i (Fig. 1 *B*).

METHODS

We solved the system (Eqs. 1 and 2) numerically, with boundary conditions described above, by using the implicit difference scheme with second-order approximation on the space grid interval, Δx, and first-order approximation on the time grid interval, Δt. The two-dimensional version of this method is based on replacing the multidimensional Laplace operator with a sequence of two one-dimensional second-order Laplace differential operators, one for the X dimension and one for the Y dimension. This method is known as the fractional-step difference method (Richtmayer, 1957). Each one-dimensional problem can be solved independently in each direction by the implicit second-order approximation difference scheme resulting in a computationally efficient method. This approach has two important advantages. The first is that it allows a larger time step while maintaining unconditional numerical stability, and the second is that being locally one-dimensional, this method significantly simplifies the approximation of the multidimensional boundary conditions while maintaining a high-order numerical approximation of differential equations.

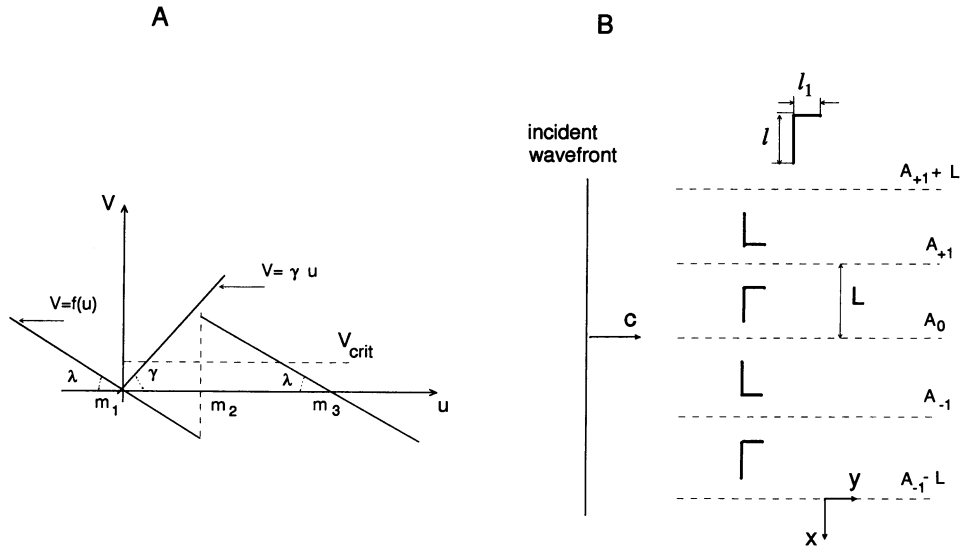

FIGURE 1 (*A*) The null-clines of the system of Eqs. 1 and 2. The function, $f(u)$, is a piecewise linear function, where the slope of each linear element, λ, refers to the rate of the fast excitation process. With respect to membrane ion channels, the function $f(u)$ corresponds to the Na current *i/v* relationship and the slope, λ, determines the maximum Na conductance and hence influences media excitability. The slope γ refers to the rate of the slow recovery process. (*B*) The relationship between the incident wavefront and a periodic lattice of inexcitable filaments. The y axis coincides with the direction of the incident wavefront. The x axis is perpendicular to the direction of the incident wavefront. Lines A_{+1} and A_{-1} correspond to a period of the lattice that is equal to $2L$.

The spatial numerical domain was a rectangular grid that did not exceed 1400 × 400 nodes in Y and X, respectively. The grid parameters were $\Delta t = 0.2$, $\Delta x = \Delta y = 0.25$. Such values of the grid parameters allowed us to keep at least four or five grid nodes per wavefront and, thus, to find a stable solution without significant influence of grid effects. Results of the two-dimensional studies were displayed with a color format so that patterns of membrane potential could be readily identified.

We studied the variations in response of the 2D lattice to single-plane wave stimuli for different values of the excitation parameter λ and relaxation parameter ϵ for constant $\gamma = 7$ and $\alpha = (m_3 - m_2)/(m_2 - m_1) = 2.75$ (see Fig. 1 *A*). Varying λ permitted us to adjust the amount of source current available for propagation and to simulate conditions associated with slow conduction secondary to Na channel blockade, high-frequency stimulation, or depolarized rest potentials.

For analytical studies, we used the singular perturbation technique with a nonasymptotic matching of $u(x,y,t)$ written in terms of a functional series for the small parameter ϵ (see Eqs. 1 and 2) (Starobin et al., 1994). We have defined a safety factor for propagation, SF, similar to that introduced by Rushton (1937) and used by Spach et al. (1981), and applied it to the boundary layer at the wavefront-obstacle interface. Written in terms of the available wavefront "source" charge, Q_S, and the charge requirements (load) of adjacent medium, Q_L,

$$SF = Q_S - Q_L. \tag{3}$$

From the resulting equation we estimated the critical value of λ, λ_{crit}, for a range of ϵ where wavefront-obstacle separation occurs, i.e., where SF = 0 with respect to the configuration of the wavefront and obstacle.

QUALITATIVE CONDITIONS FOR WAVELET FORMATION

We hypothesize that wavefront-obstacle separation is necessary for wavelet formation. To demonstrate this, we first consider the likelihood of wavelet formation when the wavefront remains attached to the obstacle after collision (Figs. 2 and 3), i.e., the medium excitability is high.

Initially, the incident wavefront collides with the inexcitable obstacle (Fig. 2 *A*, *a* and *b*). Because the boundary conditions for the obstacle are "no flux" boundary conditions (i.e., $\partial u/\partial n = 0$, where n is normal to the obstacle boundary), the flow of charge at the wavefront-obstacle interface is directed parallel to the obstacle boundary, resulting in propagation parallel to the boundary. If the propagation vector were directed away from the obstacle boundary, separation would occur. Consequently, the wavefront tips associated with the two parent wave fragments propagate toward each other following a path along the obstacle boundary (Fig. 2 *A*, *c–d*). As the two wave fragments approach each other, a small region will be "pinched off" (*e–f*). After pinch-off, the parent wavefront fragments collide and reattach. The residual excited regions attached to the obstacle propagate toward each other, eventually extinguishing propagation (*f–h*).

Fig. 3 illustrates a similar sequence of events where the vertical component of the obstacle has been extended. In this case, a large "pocket" of excited medium remains after the "pinch-off" of the curled, daughter segment of the parent wavefront (*f*). Note the polygon-like object formed by the daughter segments and the obstacle boundary. The velocity vectors at all points along the daughter wave fragments that define the boundary of this polygon are directed "inward" toward the excitable medium. Because each daughter fragment propagates toward the interior of this region (*f–j*), escape to excitable medium outside this enclosed region is not possible. The "attachment" of the wavefront to the obstacle boundary maintains "virtual" continuity, thus eliminating the possibility of wavelet "birth." In other words, a "classical" wavebreak in the Balakhovsky-Krinsky sense is not created after collision of the wavefront and the obstacle. Note that this argument is true only when the medium is homogeneous (except for the presence of inexcitable obstacles). If there are spatial differences in refractory properties as used in the original Krinsky model (1966), then there may be conditions that permit "escape."

In contrast, when the excitability of the medium is reduced, the "parent" wavefront separates from the obstacle (Fig. 2 *B*, *b*) and the right fragment end begins to curl because of the increased load "seen" by the tip region. The vertical element of the L obstacle acts to prevent curling of the left attached fragment, creating an asymmetry in spiral development that reduces the spatial requirements for fragment formation (*c–e*). In concert with curling, the tip regions of both parent fragments also propagate toward each other and eventually collide (*f*). As the curled regions of the two parent fragments collide, a small "daughter" fragment resulting from the asymmetric development of the two parent fragments is "pinched off" (*g*) and propagates approximately perpendicular to the parent propagation vector (*h*). This daughter fragment becomes the source of a new wavelet. We will now concentrate our analysis on the conditions for wavefront-obstacle separation before wavelet "birth."

ANALYTICAL CONDITIONS FOR WAVEFRONT SEPARATION FROM THE OBSTACLE

Let us consider the collision between a plane excitation wave and an inexcitable obstacle. For analytical simplicity, we will consider the element parallel to the x axis of the L-shaped obstacle, which is formed by a straight long ($l \gg L_f$) and narrow ($d < L_f$) filament and aligned parallel to the wavefront (Fig. 4 *A*). Here L_f is the wavefront thickness. Therefore, one can assume that wavefront-obstacle separation depends only on the behavior of the medium within a small region that is on the order of L_f and located near the

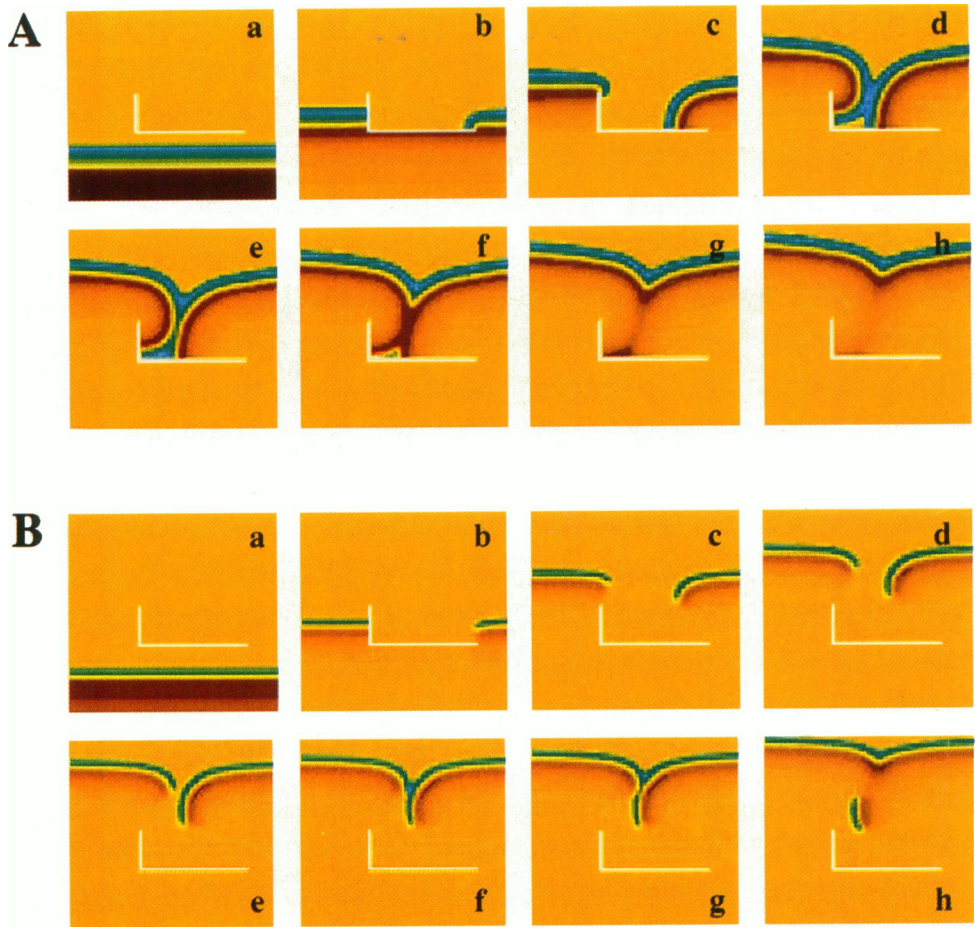

FIGURE 2 Wavefront-obstacle interactions for safety factors near zero. The temporal evolution of the wavefront is shown in frames from left to right, top to bottom. The membrane potential is color coded: the orange background in all frames refers to the rest potential $u(x,y,t) = m_1$; the red shadows represent the area of membrane recovery; the green region represents the excitation zones. (*A*) When the safety factor is positive so that $\lambda > \lambda_{crit}$, then the charge in the wavefront segments adjacent to the obstacle is adequate to excite all of the medium between the wavefront tips and the obstacle. The model parameters were $\lambda = 0.9$; $\epsilon = 0.018$; $\gamma = 7$; $\alpha = 2.75$. Under these conditions, there is no wavefront-obstacle separation. After the two wave fragments rejoin (bottom sequence of frames), the "pinched-off tail" dies because the velocity vectors of the residual wave fragments are directed toward refractory media. (*B*) The reverse phenomenon: wavefront-obstacle separation and formation of a daughter wavelet. In this case, we reduced $\lambda = 0.738 = \lambda_{crit}$, so that the SF = 0. With this choice of parameter, there is insufficient charge in the wavefront tip to excite all of the medium between the tip and the obstacle border so that the wavefront separates from the obstacle and begins to curl. After reattachment of the two parent fragments (*bottom sequence of frames*), a daughter wavelet is "pinched off" from the parent wavefront and propagates in a direction that is approximately perpendicular to that of the parent wavefront. Note that the reduction in λ results in a shorter wavelength, indicating slower propagation.

corner of the filament. Under these conditions, the analysis can be considered to be quasi-one-dimensional.

Earlier we showed that if the wavefront thickness L_f is less than L_{crit} (the maximum wavefront thickness necessary for propagation at zero velocity), there is insufficient charge available in the wavefront to support propagation in a homogeneous medium. Consequently, our analysis will assume medium properties such that $L_f > L_{crit}$ (Starobin et al., 1994).

In a highly excitable medium the ends of a wave fragment are able to excite adjacent medium such that they can turn around the corners of the obstacle, slip along its surface, and recombine to reestablish the incident wavefront. As excitability is reduced (a smaller safety factor), the fragment ends are progressively less able to excite adjacent medium, thus reducing the coupling with the surface of the obstacle. As the excitability is further reduced, the tip velocity will become negative and a portion of the wavefront will withdraw from the obstacle boundary (Mikhailov and Zykov, 1991). The transition value of the excitability where a wavefront separates from the obstacle is determined by the critical wavefront thickness, $L_{fc} > L_{crit}$. L_{fc} is determined when SF = 0, which reflects the balance of "charge" available within the wavefront adjacent to the obstacle boundary and the amount of charge necessary to form an impulse that accelerates from $C = 0$ to C_{crit}. This approach has been developed by Zeldovich et al. (1985) and modified by Starobin et al. (1994).

We assume that wavefront separation evolves within a small region of order L_{fc}. Because we can neglect the changes of wavefront thickness that are less than L_{fc}, we assume that separation occurs in a square transition region

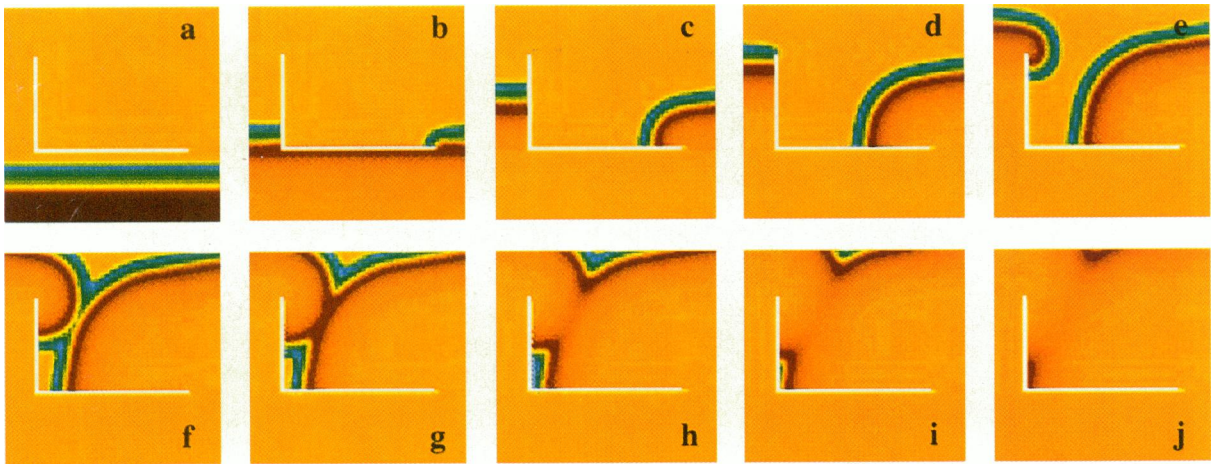

FIGURE 3 Similar to Fig. 3, this sequence of frames illustrates the fate of daughter fragments when the media excitability is adequate to maintain wavefront-obstacle attachment, i.e., $\lambda = 0.9$; SF > 0. In this illustration, the vertical arm of the "L" obstacle has been extended to demonstrate the nature of daughter wavelet annihilation after "pinch-off" from the parent wavefront. The no-flux boundary conditions at the obstacle boundary ($\partial u/\partial n = 0$) ensure that propagation of the daughter fragments at the obstacle boundary is parallel with the boundary. This condition ensures that the velocity vectors of each residual wave fragment (*bottom sequence of frames*) point toward refractory media. As shown, the polygon enclosed by the daughter wavelets eventually collapses.

with a side of L_{fc} (Fig. 4 *B*). Separation occurs if the portion of the transition region adjacent to the corner of the obstacle has a zero (in both X and Y directions) propagation velocity associated with a critical value of a wavefront thickness, L_{crit}.

Integrating Eqs. 1 and 2 over the transition region and time interval Δt, one can find that the source amount of charge, $Q_S = (m_3 - m_1)\Delta t\,(L_{fc})^2/2$, produced in the transition region (source charge) during the time interval Δt. The factor of 2 arises from our assumption that the wavefront velocity in the Y direction decreases linearly from C_{crit} to 0 (so we use $C_{crit}/2$), whereas in the X direction the velocity is 0. The load charge is equal to the sum of the charge flowing into the two leading wavefronts (this charge is approximated by the gradient over the distance, L_{crit}), $Q_{LW} = 2L_{crit}\,(m_3 - m_1)\Delta t/L_{crit}$, and the charge required for wavefront acceleration from $C = 0$ to $C = C_{crit}$ of the two developing wavefronts (approximated by square impulses of size, L_{crit}) propagating in both X and Y directions, $Q_{LR} = 2(L_{crit})^2\,(V_{eq} - V_{crit})\Delta t$. Under normal conditions of propagation, the time constant of the slow process is much greater than the time constant of the fast process, so that this term is zero (i.e., the medium in the region of the developing wavefronts is at V_{eq}). However, during early impulse development when the wavefront velocity is near zero, the time constants are comparable (Ostrovskii and Yakhno, 1975), so that the "slow" current cannot be ignored. We have conservatively estimated this charge requirement in terms of the gradient, $V_{eq} - V_{crit}$. With these components, we can write the equation for SF as

$$\mathrm{SF} = Q_S - Q_L = Q_S - (Q_{LW} + Q_{LR})$$
$$\mathrm{SF} = \tfrac{1}{2}(m_3 - m_1)L_{fc}^2 - 2(m_3 - m_1) - 2(V_{eq} - V_{crit})L_{crit}^2. \quad (4)$$

Here V_{eq} is the equilibrium level of a slow recovery current, and V_{crit} and L_{crit} are the critical values of a slow current and a wavefront length associated with a zero propagation velocity, respectively. According to the assumptions mentioned above, these values can be found from the 1D theory described in (Starobin et al., 1994)

$$b_1 = -0.5C_0 + (0.25C_0^2 + \lambda)^{1/2},$$
$$b_2 = 0.5C_0 + (0.25C_0^2 + \lambda)^{1/2}$$
$$G = \left(\frac{b_2}{b_1}\right)^{b_1/(b_1+b_2)} + \left(\frac{b_2}{b_1}\right)^{-b_2/(b_1+b_2)}, \quad K = (m_3 - m_1)/G \quad (5)$$
$$L_f = \ln(M^{-1}K)\frac{b_1 + b_2}{b_1 b_2}, \quad L_{crit} = 2\ln(M^{-1}K)/\sqrt{\lambda}$$
$$V_{eq} = V_{crit} - \lambda(m_2 - m_1)\frac{\alpha - 1}{2}.$$

Here C_0 is a wavefront propagation velocity in a 1D excitable cable which (for $f(u)$ shown in Fig. 1 and $\epsilon = 0$) is given by

$$C_0 = (\alpha - 1)(\lambda/\alpha)^{1/2} \quad (6)$$

where

$$\alpha = (m_3 - m_2)/(m_2 - m_1)$$

The factor M is a small constant that defines the threshold of u, relative to m_1 $(m_1 + M)$ and m_3 $(m_3 - M)$, associated with the wavefront boundaries.

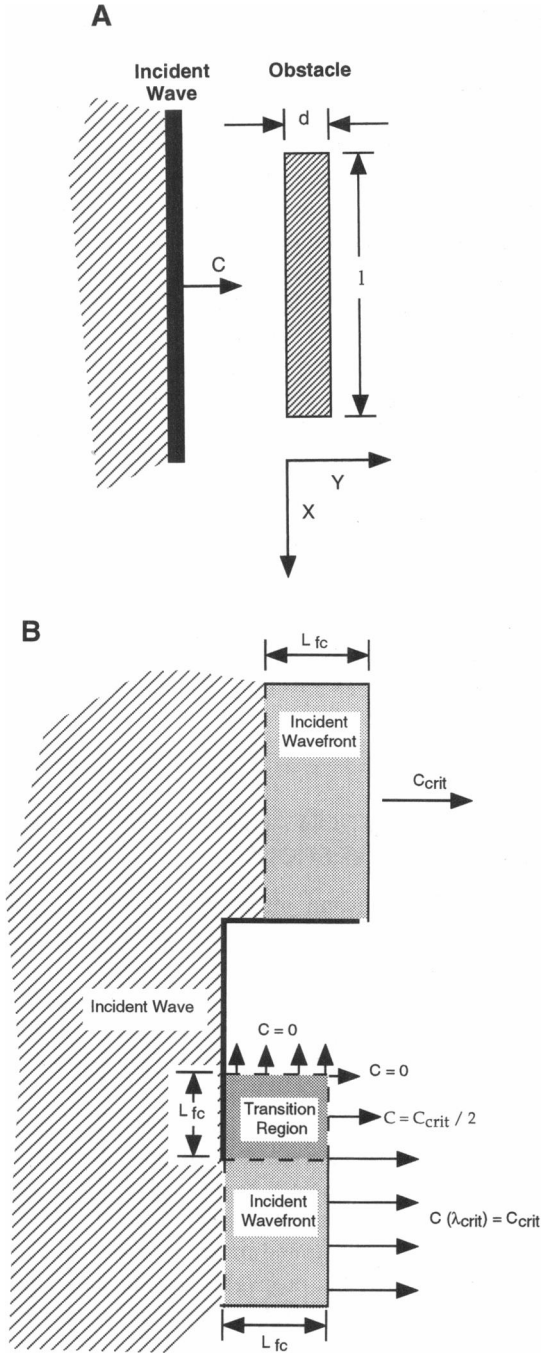

FIGURE 4 The boundary layer between a plane wavefront and an inexcitable obstacle. (*A*) Orientation of the plane wave relative to the inexcitable obstacle of length l and thickness d. (*B*) Areas of the wavefront and the obstacle that are considered in the analysis of separation. The incident wavefront of thickness, L_{fc}, supplies charge to the transition region of similar thickness. The transition from wavefront-obstacle attachment to wavefront-obstacle separation occurs when SF = 0, i.e., when the charge available from the incident wavefront is equal to the charge requirements necessary to excite all of the media within the transition region. The parent wavefront velocity C_{crit} and the critical wavefront length L_{fc} associated with transition from wavefront-obstacle attachment to wavefront-obstacle separation reflect properties of the wavefront when SF = 0 at the wavefront-obstacle boundary.

Taking into consideration that the factor G in Eq. 5 is insensitive to the propagation velocity C_0, and substituting Eq. 5 into Eq. 4, we get

$$\frac{SF}{L_{crit}} = \sigma\left(\frac{c^2}{8\lambda} + \frac{1}{2}\right) - \lambda\left(\frac{1}{2\sigma} - \sigma\frac{\alpha - 1}{\alpha + 1}\right)$$
$$\sigma = \ln\left(M^{-1}(m_3 - m_1)/2\right) \tag{7}$$

In a zero-order approximation of ϵ (singular limit, $\epsilon = 0$) the wave propagation velocity C is equal to C_0, but adding the first-order term reduces the velocity: $C = C_0(1 - \zeta_0\epsilon)$ (Mikhailov, 1990). It was shown by Starobin et al. (1994) that the wavefront propagation velocity of the peak of the wavefront, $C(V^*)$, is given by

$$C(V^*) = C_0(V_{eq})(1 - \zeta_0\epsilon), \quad V^* = V_{eq} - \epsilon\gamma(m_3 - m_1)\tau \tag{8}$$

where $C_0(V_{eq})$ is the propagation velocity of a trigger wave where recovery is absent, V^* represents the value of the recovery current at the peak of the wavefront, and $\tau\sigma = L_f(C_0)/C_0$ is the front formation time. Using Eqs. 5 and 6, one can find ζ_0, keeping the linear term in Taylor's expansion of $C(V^*)$ near $C_0(V_{eq})$,

$$\zeta_0 = \gamma(\alpha\lambda)^{-3/2}\frac{(\alpha + 1)^4}{\alpha - 1} \tag{9}$$

Substituting Eqs. 8 and 9 into Eq. 7, we find the equation for SF in terms of medium parameters and the roots of $f(u)$

$$\frac{SF}{L_{crit}} = \left[1 - \frac{1}{2\sigma^2}\frac{\alpha + 1}{\alpha - 1}\right]\lambda^3 + \frac{(\alpha + 1)^3}{8\alpha(\alpha - 1)}\lambda^2 - \epsilon\frac{\gamma(\alpha + 1)^5\sigma}{8\alpha^2(\alpha - 1)} \tag{10}$$

Here we see that the transition between wavefront-obstacle separation and wavefront-obstacle attachment (i.e., SF = 0) can be altered by varying any of the medium parameters. Because of the link between λ and the sodium current i/v relationship in excitable cells, we have chosen to focus our analyses on conditions where $\lambda = \lambda_{crit}$, where λ_{crit} is a root of the equation SF = 0 (Fig. 5 *A*).

Because $\sigma > 1$ and $\epsilon > 0$, Eq. 10 has a single positive real root, λ_{crit} when SF = 0. When $\lambda > \lambda_{crit}$ then SF > 0, and propagation at the wavefront-obstacle boundary succeeds, whereas when $\lambda < \lambda_{crit}$, then SF < 0 and local propagation fails at the obstacle-wavefront interface and wavefront-obstacle separation occurs (Fig. 5 *A*). As we indicated in the introduction, depolarization of the membrane potential, Na channel blockade, and high-frequency stimulation all reduce Na channel availability, equivalent to reducing λ. This results in a reduction of the SF because the available wavefront "source" charge, Q_s, decreases. Fig. 5 *A* shows that the smaller the value of λ, the smaller the SF. It is important to point out here that the safety factor we have defined above is a "local" property and is determined by the interaction between a local source and load presented by the obstacle-wavefront interface as indicated in our approximations.

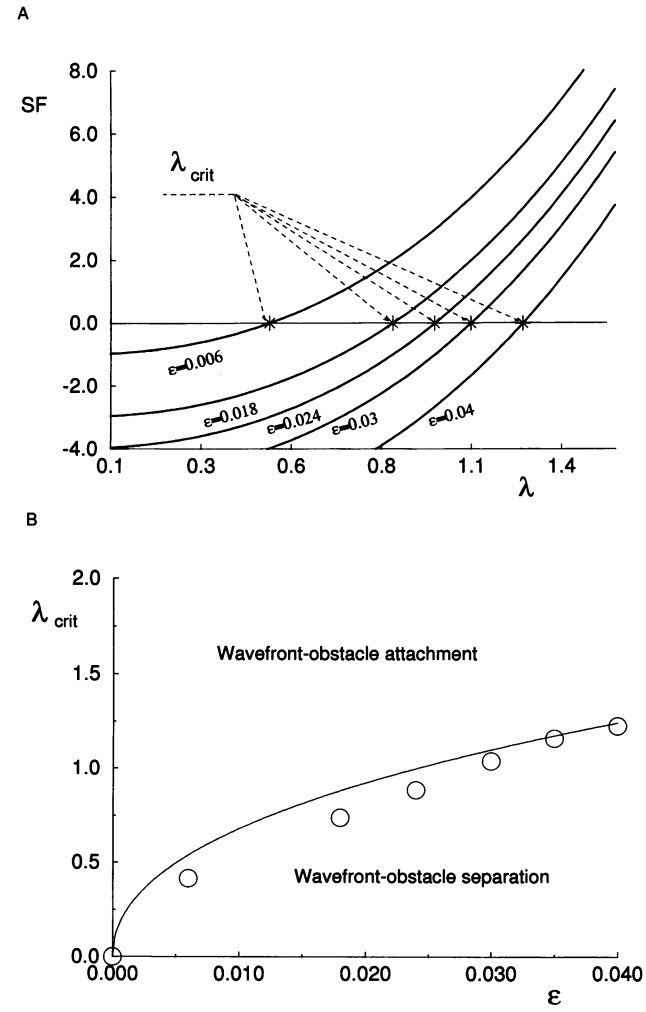

FIGURE 5 (*A*) The relationship between λ and SF/L_{crit}. Shown are theoretical plots of the safety factor (SF, Eq. 10)) as a function of λ and ϵ when $\gamma = 7$. Note that as ϵ is increased (decreasing excitability), λ_{crit}, defining the transition between wavefront-obstacle separation and wavefront-obstacle attachment, also increases, indicating the increased charge requirements necessary for propagation into less excitable media. (*B*) The dependence of the critical slope of $f(u)$ for wavefront-obstacle separation, λ_{crit}, as a function of the model parameter ϵ while $\gamma = 7$. The solid line represents the analytical approximation of λ_{crit} (root of SF = 0), and the circles represent numerically determined values. The curve of λ_{crit} as a function of ϵ separates the plane into a region where wavefront-obstacle separation occurs (below the curve) and where wavefront-obstacle attachment is maintained (above the curve). The numerical experiments reveal good agreement with the analytical approximation.

To compare the numerical solution of Eqs. 1 and 2 and analytical results given by Eq. 10, it is necessary to define factor M (Eq. 7) designating the boundaries of a wavefront. The precision of our numerical results is bounded by $M = \eta(\Delta t + \Delta x^2) = \max(i,j,n)|u_{i\Delta x,\ j\Delta y,\ n\Delta t} - u_{exact}(x,y,t)|$. We used this quantity as a threshold for defining the beginning and the end of a wavefront. Here $u_{exact}(x,y,t)$ is the exact solution of Eqs. 1 and 2, and i_0, j_0, and n_0 are the grid parameters, with $1 \le i \le i_0$, $1 \le j \le j_0$, $1 \le n \le n_0$. Our numerical experiments found that η is equal to 1.12, making M equal to 0.293 ($M = 4.688\Delta x^2$). The values of grid intervals used for all numerical experiments were $\Delta t = 0.2$ and $\Delta x = \Delta y = 0.25$.

With the value of M determined, we evaluated the accuracy of λ_{crit} derived from the roots of SF = 0 (Eq. 10) by estimating numerically the critical value of λ associated with the transition from wavefront-obstacle attachment to wavefront-obstacle separation using numerical experiments. We set $\gamma = 7$, selected a value of ϵ and then numerically solved the FHN equations (Eqs. 1 and 2) for different values of λ using a binary search. We terminated the search when the difference between two successive estimates of λ associated with wavefront-attachment and separation was <0.01. Fig. 5 *B* illustrates the theoretical predictions (Eq. 10) and the numerically determined values (*circles*). These experiments revealed good agreement with Eq. 10 for values of $\epsilon < 0.04$, comparable to physiologic conditions reflecting a 25-fold difference between the excitation and recovery time constants. For smaller ϵ when $C_{crit} < 1$, our numerical results illustrate a departure from the theoretical curve because the linear approximation of the front formation time $\tau\sigma = L_f(C_0)/C_0$ in Eq. 7 is valid only for $C_{crit} = O(1)$ (Starobin et al., 1994).

WAVELET EVOLUTION AND INSERTION BEHIND THE PARENT WAVEFRONT

Wavefront formation and insertion is a function of both wavefront-obstacle interactions and wavefront-wavefront collisions. Here we will illustrate the role of wavefront-wavefront collisions in the insertion process. Because of the mirror symmetry of the L obstacles in the lattice, it is helpful to follow the evolution of paired wavelets as shown in Fig. 6 for several lattice elements.

After collision of the parent wavefront and the obstacle (Fig. 6, *b–c*), attached (a) and unattached (u) wavefronts develop. Next the daughter wavelets (labeled d in frame *d*) are "pinched off" as a result of reattachment of the parent wave fragments (as illustrated in detail in *e–h* of Fig. 2 *B*). These daughter wavelets propagate toward each other in a direction that is approximately perpendicular to the parent propagation vector (Fig. 6, *d–e*). After collision of the daughter fragments at the lines of symmetry, A_{+1} and A_{-1}, residual wavelets develop that propagate antegrade to the parent wavefront, and their end points begin to curl (Fig. 6, *f–g*). The final event in the insertion process is the collision shown in frame *h* resulting in reattachment of adjacent fronts. With our choice of obstacle and lattice dimensions, new secondary daughter wavelets arise along the $A_{-1} - L$, A_0, and $A_{+1} + L$ lines of symmetry (Fig. 6 *h*) that lead to a repetition of the insertion process as illustrated in Fig. 7.

The growth of the two wave fragments shown in Fig. 6, *f–h*, reflect what we have labeled as "insertion," that is, a new wave front has been inserted behind the parent wave, increasing the apparent frequency of excitation of a region in front of the parent. Moreover, it is now possible to

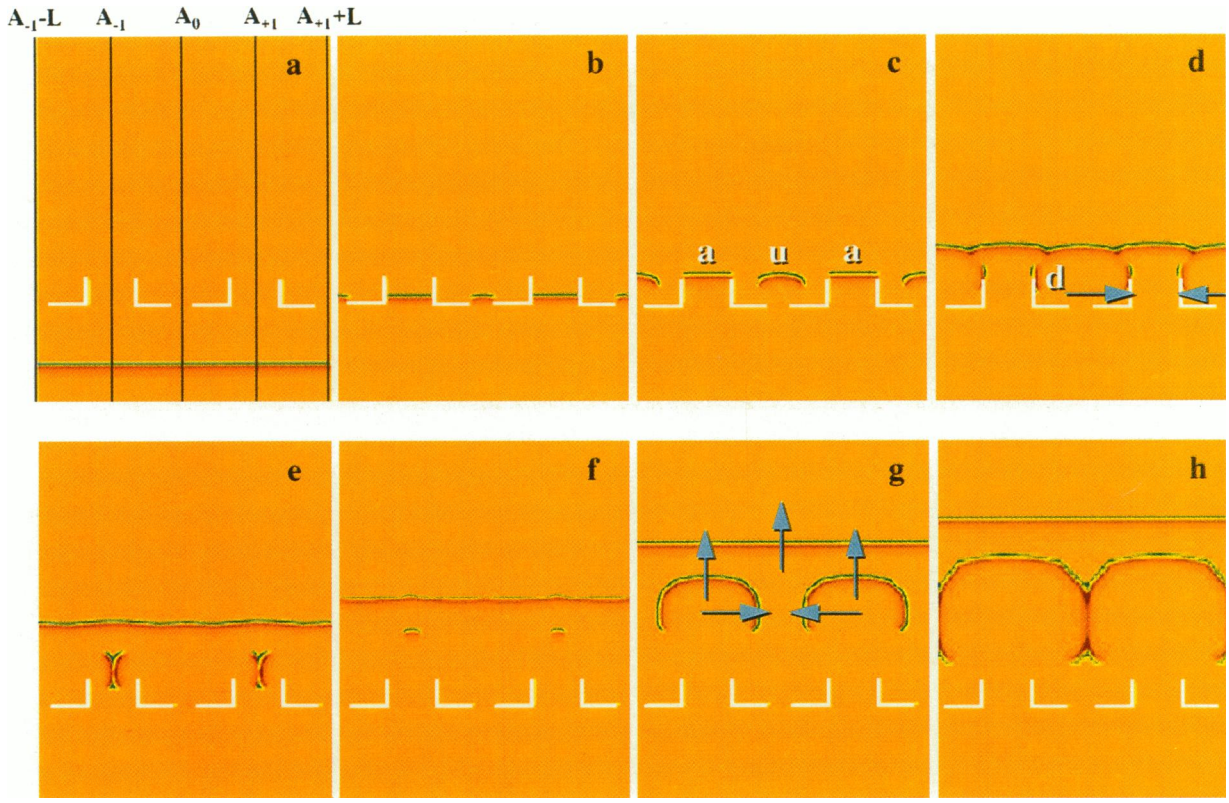

FIGURE 6 The development of secondary waves and insertion behind the incident wave (SF = 0). The orange background in all frames refers to the rest potential $u(x,y,t) = m_1$; the red shadows represent the area of membrane recovery; the green region represents the excitation zones. The inexcitable obstacle is shown in white. Time increases, left to right, top to bottom (*a–h*). The medium is initially excited behind the obstacle in *a*. The break of the parent wavefront shown in *a* is followed by propagation of an attached (a) wave fragment and unattached (u) wave fragment (*b-c*). The ends of the unattached fragment begin to curl, daughter (d) fragments are "pinched off" and propagate toward the A_{+1} and A_{-1} lines of symmetry (*c–e*). Simultaneously, the parent wavefront is restored (*d*). After collision of the daughter wavelets (*e*), residual secondary excitation zones (new wavelets) begin to grow around the A_{+1} and A_{-1} lines of symmetry (*f* and *g*). These wavelets propagate both antegrade to the parent wavefront and toward the A_0 line of symmetry (*g*), where they collide (*h*) and the insertion behind the restored parent wavefront (*f–h*) is completed. The model parameters were $\lambda = 0.738 = \lambda_{crit}$; $\epsilon = 0.018$ and $\gamma = 7$, $\Delta t = 0.2$.

visualize a mechanism for increasing the frequency of the post-obstacle wave train. If the post-obstacle train were the result of a single rotating spiral (in the absence of obstacles), then the time between successive wavefronts would be equal to the time required for one spiral revolution. In contrast, the time required for insertion of a new wavefront using interfering wavelets is approximately one-fourth the revolution time of a single spiral. As we will see in the next section, the lattice spacing can lead to two daughter wavelets arising between each pair of obstacles (Fig. 7 *c*) that will further double the insertion rate.

MULTIPLE WAVEFRONT INSERTIONS BEHIND THE INCIDENT WAVEFRONT

The final stage of our study was to demonstrate how high-rate excitation of a region of excitable medium in front of the lattice is continued in the absence of additional stimulation. This is accomplished by rapidly creating and inserting new wavelets behind the original incident wavefront. Above, we illustrated insertion of the first new wavefront behind the parent wavefront. Here we illustrate the role of the lattice and obstacle dimensions in creating interference patterns that permit rapid additional wavelet formation and insertions.

Although we consider the events after a single incident wavefront, our study approximates the clinical setting where the excitation rate may be low (SA node rate of 1/s). It is important to note that the combination of low-excitability and low-frequency periodic stimulation results in a large excitable gap (i.e., the wavelength is much less than the distance between wavefronts initiated by stimulation), so that insertion of additional wavefronts is feasible. Recent studies of regional excitability during atrial fibrillation revealed that the reentry circuits do contain excitable gaps, allowing regional control of atrial fibrillation by local external stimulation (Kirchhof et al., 1993).

In our model, the collision of wavelets near the lines of symmetry results in fragments that can potentially be inserted behind the parent wavefront. The wavelet multiplication results from repeated wavelet spawning along the $A_{+1} + L$, A_0, and $A_{-1} + L$ lines of symmetry as illustrated

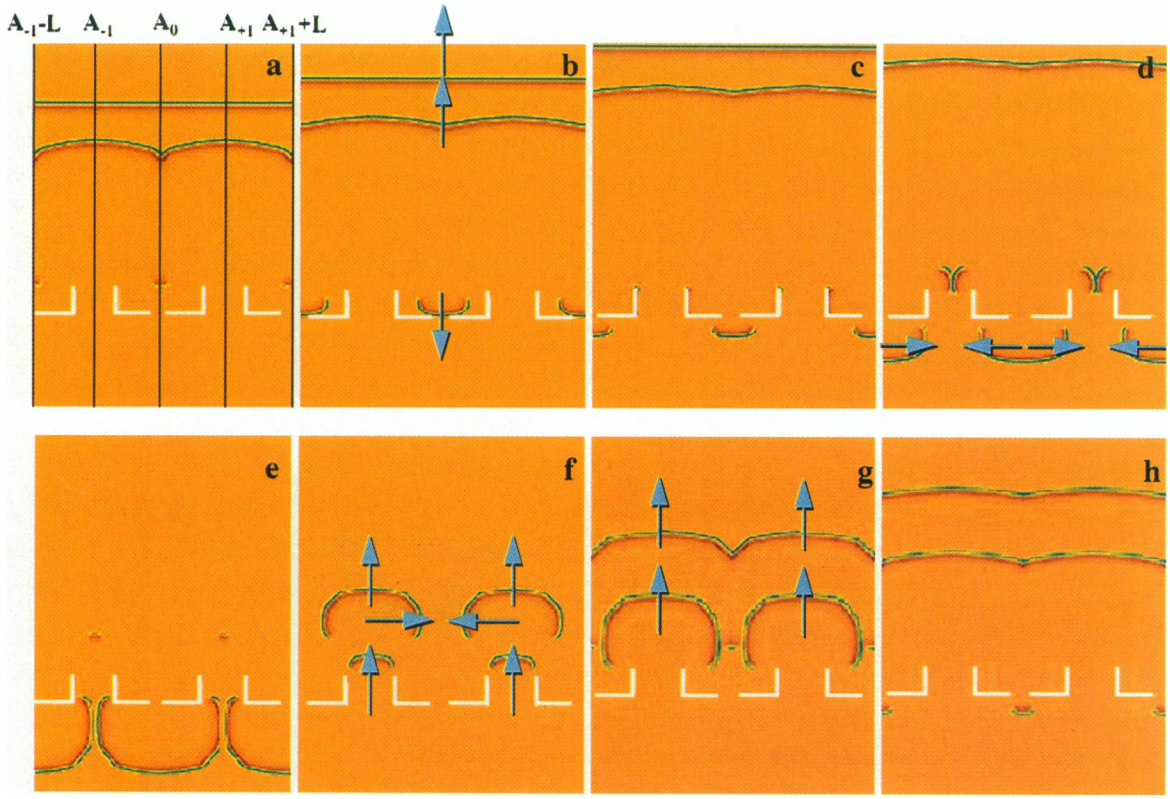

FIGURE 7 This sequence of frames (*left to right, top to bottom*) is a continuation of the events shown in Fig. 6 and highlights the sequence of events leading to multiple wavefront insertion. Note that in Fig. 6, the wavelets that are eventually inserted behind the parent wavefront are located at the A_{+1} and A_{-1} lines of symmetry (Fig. 6 *f*). After insertion and collision of the curled regions (Fig. 6 *g–h*), residual fragments remain at the $A_{+1} + L$, A_0 and $A_{-1} + L$ lines of symmetry, which become the new wavelet generators. Fig. 7 illustrates the development of these fragments. Note that first, the residual fragments propagate retrograde to the parent and inserted wavefronts (*b*). These wavelets collide with the obstacles, resulting in paired new zones of excitation (*c*) that propagate toward the A_{-1} and A_{+1} lines of symmetry (*d*). The wavelets above the obstacle collide while the wavelets below the obstacle grow and collide (*e*). Now the process shown in Fig. 6 is repeated. The residual daughter wavelets (developed both in front of and behind the obstacle) propagate antegrade to the parent wavefront (*f* and *g*) and eventually join, completing the insertion process. Note that in this illustration, the obstacle and lattice semiperiod dimensions are such that two new wave fragments are formed that are eventually inserted behind the parent wave.

in Fig. 6, *c–f*, and Fig. 7, *b–e*. Fig. 7 *a* illustrates the first repetition of residual wavelet development near the obstacle at the $A_{+1} + L$, A_0, and $A_{-1} - L$ lines of symmetry (shown in Fig. 6 *h*). These wavelets propagate retrograde to the parent wavefront and collide with the obstacle (Fig. 7, *b–c*). In this case, two daughter fragments are born (Fig. 7 *c*), one that propagates behind the obstacle and one that propagates within the obstacle and escapes. As these two pairs of new fragments grow, they collide with their symmetrical partner around the A_{+1} and A_{-1} lines of symmetry (Fig. 7, *d–e*) and the residual wavelets propagate antegrade to the parent wavefront, developing into two newly inserted wavefronts (Fig. 7, *f–h*).

In this example, wavelet multiplication and insertion is dependent on the obstacle and lattice dimensions. Shown in Fig. 8 are the relationships between the critical slope of $f(u)$, λ_{crit}, the minimal lattice semiperiod (L_{min}), and the minimum horizontal length of the obstacle (l_{min}) for wavelet formation and subsequent interference leading to insertion. λ_{crit} was computed as a function of ϵ when $\gamma = 7$. Obstacle lengths $< l_{min}$ provide insufficient area for the pinched-off wavelet to develop subsequent to "pinch-off" (Fig. 6, *c–d*). Similarly, lattice semiperiods $< L_{min}$ provides insufficient space for wavelet development such that subsequent to collision, an inserted wavelet is born (Fig. 6 *f*).

The rate of insertion is also dependent on λ_{crit}. Fig. 9 shows the rate of insertion per dimensionless time unit. The larger λ_{crit} (indicating large ϵ; Fig. 5, *A* and *B*), the shorter the time interval required for paired fragments initiated near symmetry lines A_{+1} and A_{-1} to reach the A_0 symmetry line (Fig. 6, *e–h*; Fig. 7, *e–h*). Similarly, the fragment initiated near the A_0 line of symmetry (Fig. 6, *b–e*; Fig. 7, *a–e*) can evolve rapidly toward the A_{+1} and A_{-1} lines of symmetry, and hence, the larger the number of additional plane waves available to be inserted behind the restored incident wavefront.

DISCUSSION

Atrial and ventricular fibrillation are significant clinical problems, yet our understanding of the mechanisms of ini-

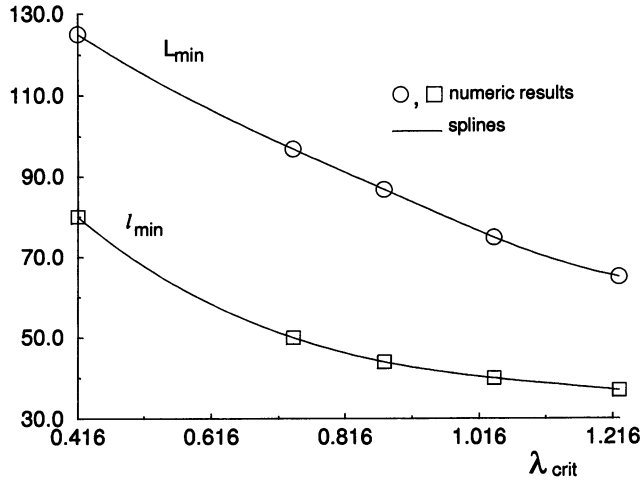

FIGURE 8 The minimal lattice and obstacle parameters as a function of the critical slope, λ_{crit}, of $f(u)$. The model parameter, ϵ, was varied, $\gamma = 7$, and λ_{crit} was computed from the roots of equation 10. Lengths are reported in dimensionless units. The minimal obstacle length, l_{min}, is the minimal length required for development of the "pinched" tail that is large enough to survive, as illustrated in Fig. 2 *B* (*g–h*) and Fig. 6 (*d*). Our numerical studies indicate that the vertical element of the obstacle should be $>l_{min}/3$. The minimum lattice semiperiod, L_{min}, is also shown as a function of λ_{crit}. This parameter determines the region within which a daughter fragment can develop before collision. Note that as λ_{crit} is increased, the dimensional requirements for effective collisions that lead to inserted fragments are reduced.

tiation and maintenance is incomplete. The pioneering work of Mines (1913), Garrey (1914), and Lewis and co-workers (1920) provided a rich base of observations supporting the concept of reentry. The theoretical work of Wiener and Rosenblueth (1946), Balakhovsky (1965), and Krinsky (1966) established theoretical conditions for the creation of

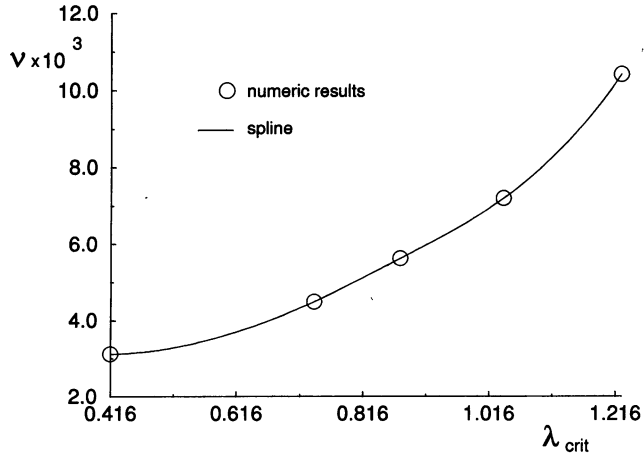

FIGURE 9 Relationship between the number of wavefronts that can be inserted behind the parent wavefront per dimensionless time unit and λ_{crit}. For these results, ϵ was varied to yield a range values of λ_{crit}. As ϵ was reduced, both the conduction velocity and wavelength of the parent wavefront were reduced, increasing the amount of medium into which new wavefronts could be inserted. The circles refer to the numeric results; the solid line is a spline.

spiral reentry, and Moe and co-workers (1962, 1964) demonstrated that multiple wavelets could evolve after high-frequency stimulation of a medium with inhomogeneous refractory properties. Recent mapping studies of Allessie (1973, 1994), Konings et al. (1994), and Boineau and Cox (1973) confirmed both multiple wavelets and reentry. In spite of the availability of a considerable body of experimental data and a theoretical basis for initiating reentry, there is relatively little theoretical or experimental work focused on the process of converting from simple reentry of a single wave of excitation to formation and multiplication of secondary wavelets. Here it is useful to note that in the majority of the experimental studies of fibrillation, slow conduction appears as a common denominator.

Balakhovsky (1965) and Krinsky (1966) showed that rupture of a wavefront (discontinuous wavefront) leads to spiral development. Later studies by Pertsov et al. (1983, 1990) though, demonstrated that a ruptured wavefront, secondary to a wavefront-obstacle collision, may not lead to spiral formation if the excitability of the medium exceeds a critical value. Using high-frequency stimulation to reduce the excitability, numerical studies by Panfilov and Keener (1993) and experimental studies in the B-Z reagent by Agladze et al. (1994) confirmed this observation. In these studies, new spiral waves evolved when the colliding wavefront separated from the obstacle. Wavefront-obstacle separation was observed to be dependent on the frequency of excitation, which resulted in attenuated excitability secondary to incomplete recovery. Although they demonstrated wavefront-obstacle separation, the underlying mechanism was not explored.

The role of excitability in spiral formation can be demonstrated without incorporating obstacles (either transient or permanent). Instead of breaking a wavefront, Kogan and co-workers (1991) showed that paired spirals could be initiated by a discontinuous wavefront formed by stimulation during the vulnerable period, a period of reduced excitability after the passage of a wavefront. Stimuli applied during the vulnerable period resulted in wavefront formation only in directions retrograde to the direction of parent wavefront propagation. Stimulation outside the vulnerable period, into recovered medium, on the other hand, resulted in continuous wavefront formation and no spiral formation.

The concept of a safety factor relating source and load charge requirements was introduced in studies of propagating wavefront nerve cells by Rushton (1937) and used to characterize propagation in an anisotropic cardiac tissue by Spach et al. (1981). A reduced safety factor can arise in certain cardiac diseases from the development of poorly conducting or nonconducting obstacles secondary to myocardial infarction (Boineau and Cox, 1973), increased atrial fibrosis associated with aging (Spach and Dolber, 1986; Spach et al., 1988), and the presence of inexcitable cells or cells with a slightly depolarized rest potential (Ten Eick and Singer, 1979). We questioned whether the interaction between an incident wavefront and a lattice of obstacles under conditions of a reduced safety factor (as defined in Eq. 3;

see Fig. 5 *A*) was adequate to explain initiation and maintenance of multiple wavelets and promotion of high-frequency arrhythmias.

The discrete nature of cell-to-cell connections can lead to alterations in the safety factor as described by Spach and co-workers (Spach et al., 1981, 1982, 1988). They explored the nature of propagation in cardiac tissue and demonstrated that at the cellular level, propagation was discontinuous and a cell's local response was sensitive to the direction of an approaching wavefront (Spach et al., 1992), indicative of alterations in the load "seen" by a cell. Moreover, they demonstrated that structural resistive discontinuities resulting in load variations as a function of the direction of a propagating wavefront might contribute significantly to the arrhythmogenic potential of a region of tissue.

Another source of reduced safety factor is due to the background Na channel (Zilberter et al., 1994), which can lead to fast Na channel inactivation secondary to depolarized rest potentials. For instance, in diseased atrial tissue, abnormalities in the balance of resting sodium and potassium conductances (Imanishi and Arita, 1987; Hordof et al., 1976; Ten Eick and Singer, 1979) resulted in a depolarized resting potential and a significant reduction in propagation velocity (Cranefield, 1975).

Sodium channel blockade can also reduce the safety factor, thereby reducing the propagation velocity and rotational frequency of spiral waves. Concern about the proarrhythmic effects of drugs that block Na channels has recently been emphasized by clinical trials (CAST Investigators, 1989) in which patients treated with Na channel blocking agents experienced a sudden death rate approximately four times greater than that of the untreated group. One explanation of these results is that unsuppressed excitations in the treated patients were more likely to initiate reentrant tachyarrhythmias, leading to sudden cardiac death, i.e., the treated patients were more "vulnerable" than the untreated patients (Starmer et al., 1991).

Recently we showed with in vitro studies that Na channel blockade was inherently proarrhythmic by prolonging the period of vulnerability during which premature stimulation produced unidirectional conduction (Starmer et al., 1991, 1992; Nesterenko et al., 1992), a precursor of reentrant cardiac arrhythmias. However, the patients that participated in the CAST study were survivors of a myocardial infarction suggesting the presence of poorly conducting regions of cardiac scar tissue. Consequently, there is the possibility that Na blockade might trigger other proarrhythmic mechanisms based on collisions between wavefronts and obstacles in a medium of low safety factor.

To probe possible arrhythmogenic properties of diseased cardiac tissue, we have studied a medium of inherent low safety factor instead of a medium of reduced excitability secondary to high-frequency stimulation. With such a medium, new wavelets could be initiated by a single incident wavefront. We hypothesized that there are spatial patterns of obstacles such that a parent wavefront arising from a single stimulation, after colliding with the lattice, can produce multiple spiral waves leading to high-frequency arrhythmias.

With periodic excitation, poor excitability will lead to an excitable gap between successive wavefronts, behind which new wavelets can be inserted, producing high-frequency tachyarrhythmias (i.e., wavelength $\ll$ distance between two successive wavefronts). Either sustained or nonsustained tachyarrhythmias might be produced by altering excitability. These conditions, approximating those observed in cardiac disease, however, have received little attention and there are no theoretical studies describing conditions promoting wavefront-obstacle separation, an essential precursor of wavelet formation.

As has been shown by many investigators, premature stimulation may be considered as a generic mechanism of reentry initiation regardless of conductivity of cardiac tissue. In normally conducting cardiac tissue, a single rotating spiral wave can result in tachyarrhythmias. In patients with structural heart disease (e.g., intercellular fibrosis) excitability can be compromised via a reduced safety factor such that high-rate arrhythmias, as revealed by the ECG, are theoretically impossible. Only with multiple wavelets can the apparent rate of the arrhythmia be increased. The question, then, is how are multiple wavelets induced?

In our model of the obstacle, the asymmetric L provides a mechanism permitting wavelet formation in a medium of cardiac dimension (by reducing the spatial requirements for wavefront development). The lattice of multiple obstacles defines the patterns of interference between pairs of adjacent wavelets and is essential for directing wavelet development and subsequent insertion behind the parent wavefront. One might reasonably question the role of symmetry in our model.

We chose to study the interaction of a wavefront and the L-shaped obstacle as a first approximation of either a filament-like obstacle seen in atrial tissue (Spach and Dolber, 1986) or as a piecewise approximation to "solid" obstacles that appear secondary to ischemia. Similarly, the lattice was selected as a first approximation of what one might call "diffuse disease." Studies of the sensitivity of wavelet formation, insertion and multiplication to the geometric structure of the obstacle, and the lattice arrangement of obstacles remain to be done.

Studies of Moe's cellular automata model (Moe et al., 1964), though, suggest that the regularity of our symmetric lattices is not essential for forming wavelets. In his model, each cell had a refractory period selected from a normal distribution of refractory periods, and the conduction time of each cell was dependent on the time since the last excitation. High-frequency stimulation was used to initiate "fibrillation." Isochronal maps indicated the presence of multiple wavelets and multiple "functional" obstacles. Linking our studies using symmetry with Moe's studies using random distributions of refractory periods indicates that symmetry is not essential for multiple wavelet formation. The symmetry, or lack of symmetry, though, probably

determines the range of the number of wavelets that can evolve.

With these ideas in mind, the development of fibrillation can be viewed as a positive feedback process. Under normal conditions, the safety factor is positive such that wavefront-obstacle separation does not occur, thus inhibiting daughter wavelet formation. Then following a single extrastimulus, conduction of the next "normal" activation wavefront is retarded. If the safety factor has been sufficiently reduced (secondary to the reduced recovery time leading to reduced sodium channel availability), then a collision between this premature wavefront and an obstacle can lead to daughter wavelets. If SF > 0, then the parent fragments will reattach and continue normal propagation (Fig. 3 *A*). If, on the other hand, SF < 0, then the parent fragments will separate from the obstacle boundaries (Fig. 3 *B*) and may become the focus of a reentrant process that will continue to collide with nearby obstacles. As these wavelets grow and collide, new wavefronts can be inserted behind the parent wavefront, thereby increasing the apparent rate of the arrhythmia, reducing the time for cellular recovery and thus further reducing the safety factor. This leads to a further slowing of conduction and an expansion of the excitable gap (because the APD* velocity is diminished), and thus the process can continue until there is a negligibly excitable gap. It is this hypothetical feedback process that can explain the appearance of very slow conducting regions in tissue that conducts at normal velocities in the absence of fibrillation (Schuessler et al., 1992, 1993; Konings et al., 1994).

Based on these concepts, it is useful to compare our results with experimental and clinical observations of atrial flutter and fibrillation. For instance, when $L_0 = 0.05$ mm and $\tau_0 = 1$ ms, which approximate conditions of low excitability ($C = 0.05$ M/s), our dimensionless minimum lattice semiperiod in Figs. 6 and 7 scales to the lengths of observed macroreentry circuits seen in atrial flutter: $L > 5$ mm and an insertion rate of 5 Hz when $\epsilon = 0.006$. Increasing ϵ to 0.04 results in microreentrant wavelets, $L \approx 2$ mm, and higher wavelet insertion rates, 6 Hz $< \nu <$ 12 Hz (Konings et al., 1994).

This qualitative agreement permits us to interpret experimental data referring to fibrillation in theoretical terms using a minimal two-variable model describing the generic properties of an excitable medium. Based on this model we theoretically studied the safety factor of propagation and the associated critical slope of the "apparent" Na conductance, λ_{crit}. These critical parameters are essential for wavefront separation from the obstacle leading to long-lived secondary wavelets. In addition, we probed the development of reentry, insertion, and wavelet multiplication. These theoretical results are compatible with the generic spatial and frequency properties of flutter and fibrillation, and may be useful in designing interventions to control life-threatening cardiac tachyarrhythmias.

This research was supported in part by HL32994 from the National Heart, Lung and Blood Institute, National Institutes of Health.

REFERENCES

Agladze, K., J. P. Keener, S. C. Muller, and A. V. Panfilov. 1994. Rotating spiral waves created by geometry. *Science.* 264:1746–1748

Allessie, M. A., F. I. M. Bonke, and F. J. G. Schopoman. 1973. Circus movement in rabbit atrial muscle as a mechanism of tachycardia. III. The "leading circle" concept: a new model of circus movement in cardiac tissue without the involvement of anatomical obstacle. *Circ. Res.* 41: 9–18.

Allessie, M. A., I. K. Konigs, and C. Kirchhof. 1994. Mapping of atrial fibrillation. *In* Atrial Fibrillation: Mechanisms and Therapeutic Strategies. S. B. Olsson, M. A. Allessie, and R. W. F. Campbell, editors. Futura Publishing, Armonk, NY. 37–49.

Balakhovsky, I. S. 1965. Several modes of excitation movement in ideal excitable tissue. *Biofizika.* 10:1063–1067.

Boineau, J. P., and J. L. Cox. 1973. Slow ventricular activation in acute myocardial infarction. A source of reentrant premature ventricular contraction. *Circulation.* 48:703–713.

Buxton, A. E., H. L. Waxman, F. E. Marchlinsky, and M. E. Josephson. 1984. Atrial conduction: effects of extrastimuli with and without atrial dysrhythmias. *Am. J. Cardiol.* 54:755–761.

Cardiac Arrhythmia Suppression Trial (CAST) Investigators. 1989. Preliminary report: effect of encainide and flecainide on mortality in a randomized trial of arrhythmia suppression after myocardial infarction. *N. Engl. J. Med.* 321:406–412.

Cox, J. L., J. P. Boineau, R. B. Schuessler, K. M. Kater, and D. G. Lappas. 1994. Surgical interruption of atrial reentry as a cure for atrial fibrillation. *In* Atrial Fibrillation: Mechanisms and Therapeutic Strategies. S. B. Olsson, M. A. Allessie, and R. W. F. Campbell, editors. Futura Publishing, Armonk, NY. 373–404.

Cranefield, P. F. 1975. The Conduction of the Cardiac Impulse: The Slow Response and Cardiac Arrhythmias. Futura Press, Mt. Kisco, NY.

Davidenko, J. M. 1995. Spiral waves in the heart: experimental demonstration of a theory. In Cardiac electrophysiology. D. P. Zipes and J. Jalife, editors. W. B. Saunders, Philadelphia. 478–488.

FitzHugh, R. 1961. Impulses and physiologic states in theoretical models of nerve membrane. *Biophys. J.* 1:445–466.

Garrey, W. E. 1914. The nature of fibrillar contraction of the heart: its relation to tissue mass and form. *Am. J. Physiol.* 33:397–414.

Hordof, A. J., R. Edie, J. R. Malm, B. F. Hoffman, and M. R. Rosen. 1976. Electrophysiological properties and response to pharmacologic agents of fibers from diseased human atria. *Circulation.* 54:774–779.

Imanishi, S., and M. Arita. 1987. Factors related to the low resting membrane potentials of diseased human atrial muscle. *Jpn. J. Physiol.* 37:393–410.

Kirchhof, C., F. Chorro, G. J. Scheffer, J. Brugada, K. Konings, Z. Zetelaki, and M. Allessie. 1993. Regional entrainment of atrial fibrillation studied by high-resolution mapping in open-chest dogs. *Circulation.* 88:736–749.

Kogan, B. Y., W. J. Karplus, B. S. Billett, A. T. Pang, H. S. Karagueuzian, and S. S. Kahn. 1991. The simplified FitzHugh-Nagumo model with action potential duration restitution: effects on 2D wave propagation. *Physica D.* 50:327–340.

Kogan, B. Y., W. J. Karplus, and A. T. Pang. 1990. Simulation of nonlinear distributed parameter systems on the connection machine. *Simulation.* 55:271–281.

Konings, K. R. S., C. J. H. J. Kirchhof, J. R. L. M. Smeets, H. J. J. Wellens, O. C. Penn, and M. A. Allessie. 1994. High-density mapping of electrically induced atrial fibrillation in humans. *Circulation.* 89:1665–1680.

Krinsky, V. I. 1966. Spread of excitation in an inhomogeneous medium (state similar to cardiac fibrillation). *Biofizika.* 11:676–683.

Krinsky, V. I. 1984. Autowaves: results, problems, outlooks. *In* Self-Organization, Autowaves and Structures Far from Equilibrium. V. I. Krinsky, editor. Springer-Verlag, Berlin. 9–19.

Leier, C. V., J. A. Meacham, and S. F. Schaal. 1978. Prolonged atrial conduction: a major predisposing factor for the development of atrial flutter. *Circulation.* 57:213–216.

Lewis, T., H. S. Feil, and W. D. Stroud. 1920. Observations upon flutter and fibrillation. Part II. The nature of auricular flutter. *Heart.* 7:191–244.

Markin, V. S., V. F. Pastushenko, and Yu. A. Chizmadzhev. 1981. Theory of Excitable Media. Nauka, Moscow.

Mikhailov, A. S. 1990. Foundations of Synergetics 1. Distributed Active Systems. Springer, Berlin.

Mikhailov, A. S., and V. S. Zykov. 1991. Kinematical theory of spiral waves in excitable media: comparison with numerical simulations. *Physica D.* 52:379–397.

Mines, G. R. 1913. On dynamic equilibrium in the heart. *J. Physiol. (Lond.).* 46:349–383.

Moe, G. K. 1962. On the multiple wavelet hypothesis of atrial fibrillation. *Arch. Int. Pharmacodyn. Ther.* 140:183–188.

Moe, G. K. 1965. Computer simulation of atrial fibrillation. *In* Computers in Biomedical Research, Vol. 2. R. W. Stacy and B. D. Waxman, editors. Academic Press, New York. 217–238.

Moe, G. K., and J. A. Abildskov. 1959. Atrial fibrillation as a self-sustaining arrhythmia independent of focal discharge. *Am. Heart J.* 58:59–70.

Moe, G. K., W. C. Rheinboldt, and J. A. Abildskov. 1964. A computer model of atrial fibrillation. *Am. Heart J.* 67:200–220.

Nesterenko, V. V., A. A. Lastra, L. V. Rosenshtraukh, and C. F. Starmer. 1992. A proarrhythmic response to sodium channel blockade: modulation of the vulnerable period in guinea pig ventricular myocardium. *J. Cardiovasc. Pharmacol.* 19:810–820.

Ostrovskii, L. A., and V. G. Yakhno. 1975. Formation of pulses in an excitable medium. *Biofizika.* 20:489–493.

Panfilov, A. V., and J. P. Keener. 1993. Effects of high frequency stimulation on cardiac tissue with an inexcitable obstacle. *J. Theor. Biol.* 163:439–448.

Pertsov, A. M., J. M. Davidenko, R. Salomoncz, W. T. Baaxter, and J. Jalife. 1993. Spiral waves of excitation underlie reentrant activity in isolated cardiac muscle. *Circ. Res.* 72:631–650.

Pertsov, A. M., E. A. Ermakova, and E. E. Shnol. 1990. On the diffraction of autowaves. *Physica D.* 44:178–190.

Pertsov, A. M., A. V. Panfilov, and F. U. Medvedeva. 1983. Instability of autowaves in excitable media associated with the phenomenon of critical curvature. *Biofizika.* 28:100–102.

Richtmayer, R. D. 1957. Difference Methods for Initial-Value Problems. Interscience, New York.

Rushton, W. A. H. 1937. Initiation of the propagated disturbance. *Proc. R. Soc. Lond. (Biol.).* 124:210–243.

Schalij, M. J., W. J. E. P. Lammers, P. L. Rensma, and M. A. Allessie. 1992. Anisotropic conduction and reentry in perfused epicardium of rabbit left ventricle. *Am. J. Physiol.* 263:H1466–H1478.

Schuessler, R. B., J. P. Boineau, B. I. Bromberg, D. E. Hand, S. Yamauchi, and J. L. Cox. 1995. Normal and abnormal activation of the atrium. *In* Cardiac Electrophysiology. D. P. Zipes and J. Jalife, editors. W. B. Saunders, Philadelphia. 543–562.

Schuessler, R. B., T. M. Grayson, B. I. Bromberg, J. L. Cox, and J. P. Boineau. 1992. Cholinergically mediated tachyarrhythmias induced by a single extrastimulus in the isolated canine right atrium. *Circ. Res.* 71:1254–1267.

Schuessler, R. B., T. Kawamoto, D. E. Hand, M. Mitsuno, B. I. Bromberg, J. L. Cox, and J. P. Boineau. 1993. Simultaneous epicardial and endocardial activation sequence mapping in the isolated canine right atrium. *Circulation.* 88:250–263.

Spach, M. S., and P. C. Dolber. 1986. Relating extracellular potentials and their derivatives to anisotropic propagation at a microscopic level in human cardiac muscle: evidence for electrical uncoupling of side-to-side fiber connections with increasing age. *Circ. Res.* 58:356–371.

Spach, M. S., P. C. Dolber, and J. F. Heidlage. 1988. Influence of the passive anisotropic properties on directional differences in propagation following modification of the sodium conductance in human atrial muscle. A model of reentry based on anisotropic discontinuous propagation. *Circ. Res.* 62:811–832.

Spach, M. S., J. F. Heidlage, E. R. Darken, E. Hofer, and C. F. Starmer. 1992. Cellular *V*(max) reflects both membrane properties and the load presented by adjoining cells. *Am. J. Physiol.* 263:H1855–H1863.

Spach, M. S., W. T. Miller, P. C. Dolber, J. M. Kootsey, J. R. Sommer, and C. E. Mosher. 1982. The functional role of structural complexities in the propagation of depolarization in the atrium of the dog: cardiac conduction disturbances due to discontinuities of effective axial resistivity. *Circ. Res.* 50:175–191.

Spach, M. S., W. T. Miller, D. B. Geselowitz, R. C. Barr, J. M. Kootsey, and E. A. Johnson. 1981. The discontinuous nature of propagation in normal canine cardiac muscle: evidence for recurrent discontinuities of intracellular resistance that affect the membrane currents. *Circ. Res.* 48:39–54.

Starmer, C. F., A. R. Lancaster, A. A. Lastra, and A. O. Grant. 1992. Cardiac instability amplified by use-dependent Na channel blockade. *Am. J. Physiol.* 262:H1305–H1310.

Starmer, C. F., A. A. Lastra, V. V. Nesterenko, and A. O. Grant. 1991. Proarrhythmic response to sodium channel blockade: theoretical model and numerical experiments. *Circulation.* 84:1364–1377.

Starobin, J. M., Yu. I. Zilberter, and C. F. Starmer. 1994. Vulnerability in one-dimensional excitable media. *Physica D.* 70:321–341.

TenEick, R. E., and D. H. Singer. 1979. Electrophysiological properties of diseased human atrium. 1. Low diastolic potential and altered cellular response to potassium. *Circ. Res.* 44:545–557.

Tyson, J. J., and J. P. Keener. 1988. Singular perturbation theory of traveling waves in excitable media. *Physica D.* 32:327–361.

Wiener, N., and A. Rosenblueth. 1946. The mathematical formulation of the problem of conduction of impulses in a network of connected excitable elements, specifically in cardiac muscle. *Arch. Inst. Cardiol. Mex.* 16:205–265.

Winfree, A. T. 1987. When Time Breaks Down. Princeton University Press, Princeton, NJ.

Winfree, A. T. 1989. Electrical instability in cardiac muscle: phase singularities and rotors. *J. Theor. Biol.* 138:353–405.

Winfree, A. T. 1991. Varieties of spiral wave behavior: an experimentalist's approach to the theory of excitable media. *Chaos.* 1:303–334.

Yamashita, T., N. Oikawa, H. Inoue, Y. Murakawa, T. Nakajima, M. Usui, K. Ajiki, S. Ohkawa, and T. Sugimoto. 1994. Slow abnormal conduction in the low right atrium: its anatomic basis and relevance to atrial reentry. *Am. Heart J.* 127:353–359.

Zeldovich, Ya. B., G. I. Barenblatt, V. B. Librovich, and G. M. Makhviladze. 1985. The Mathematical Theory of Combustion and Explosions. Consultants Bureau, New York.

Zilberter, Y. I., C. F. Starmer, J. Starobin, and A. O. Grant. 1994. Late Na channels in cardiac cells: the physiological role of background Na channels. *Biophys. J.* 67:153–160.

Zykov, V. S. 1988. Modelling of Wave Processes in Excitable Media. Manchester University Press, Manchester.